Numerical Analysis of a Leading Edge Tubercle Hydrofoil in Turbulent Regime

Blanca Pena[1]†, Ema Muk-Pavic[1], Giles Thomas[1] and Patrick Fitzsimmons[1]

[1]Department of Mechanical Engineering, University College London, London, WC1E 7JE, UK

(Received xx; revised xx; accepted xx)

This paper presents a numerical performance evaluation of the leading edge tubercles hydrofoil with particular focus on fully turbulent flow regime. Efforts were focused on the setting up of an appropriate numerical approach required for an in-depth analysis of this phenomenon, being able to predict the main flow features and the hydrodynamic performance of the foil when operating at high Reynolds numbers. The numerical analysis was conducted using an Improved Delayed Detached Eddy Simulation (IDDES) for Reynolds numbers corresponding to transitional and fully turbulent flow regimes at different angles of attack for pre-stall and post stall regimes.

The results show that tubercles operating in turbulent flow improve the hydrodynamic performance of the foil when compared to a transitional flow regime. Flow separation was identified behind the tubercle troughs, but was significantly reduced when operating in a turbulent regime and for which we have identified the main flow mechanisms. This finding confirms that tubercle effect identified in transitional regime is not lost in a turbulent flow. Furthermore, when the hydrofoil operates in turbulent flow regime, the transition to a turbulent regime takes place further upstream. This phenomenon suppresses a formation of a laminar separation bubble and therefore the hydrofoil exhibits a superior hydrodynamic performance when compared to the same foil in transitional regime. The analysis approach presented here proved to be capable to accurately assess flow characteristics needed to determine the flow changes required in order to match with appropriate tubercled energy saving device design resulting in favorable flow changes.

1. Introduction

Looking into nature one can find some outstanding inventions that have been a result of millions of years of evolution. Engineers often look there to find inspiration for modern technological solutions. In this paper a work that is inspired by the flippers of the humpback whale will be presented. These large mammals are known to have excellent hydrodynamics capabilities, in particular for maneuvering. They are fast and agile and that can be partially attributed to a specific shape of their flippers. While for most of the sea mammals flippers are shaped as smooth hydrofoils, the flipper's leading edge of the humpback whale has a series of "bumps" called tubercles. Ongoing research has been focused in understanding the action of these tubercled foils to see if they can be successfully implemented in engineering design.

Such tubercles were first researched and described as natural lift enhancement devices by Fish and Battle (1995) who recognized that the presence of tubercles on a flipper can delay the stall, allowing the flipper to maintain a high lift coefficient at the high angles of attack. Other researchers looked at the impact of the shape on the performance of

† Email address for correspondence: blanca.pena.16@ucl.ac.uk

the humpback whale flipper. For example, Miklosovic et al. (2004) experimentally tested three flipper shapes with and without tubercles. They found that, by the introduction of tubercles, an increase in the maximum produced lift and in the stall angle was achieved. It was also found that at certain angles of attack the drag decreased as well. In addition, Miklosovic et al. (2007), concluded that tubercle behaviour is dependent on wing overall shape as well. Likewise, Johari et al (2007) conducted the experimental evaluation of NACA shaped section wings with a smooth leading edge (without tubercles) and with leading edge tubercles having a range of the tubercle wave amplitude (see Figure 1b). They highlighted that the best hydrodynamic performance was achieved by the foil with the smallest wave amplitude.

Although previous research showed a strong dependence on tubercle geometry and foil shape, as expected the main factor affecting the performance of tubercled foils is the Reynolds number (Re). Stanway (2008) presented experiments for a half-span model at different Reynolds numbers ranging from 4×10^4 and 1.2×10^5 . Stanway indicated that at the highest Reynolds number the maximum achieved lift coefficient was significantly higher than at lower Reynolds number. Direct numerical simulations (DNS) of the flow over leading edge tubercled foils at low Reynolds numbers of 10^4 and 5 x 10^4 (Serson et al.,2017) revealed that at the higher Reynolds number a transition from laminar to turbulent flow regime is happening further upstream. Rostamzadeh et al (2017) looked into the tubercled wing's performance in a transitional-near turbulent regime. It was observed that tubercled foils produce a lower drag coefficient at high, rather than at low, Reynolds Numbers.

Most of the research presented above was experimental with some attempting to numerically model leading edge tubercle flow. The first numerical simulations were conducted by Watts et al. (2001), who used a panel method for the flow continua calculations. However, panel method considers an inviscid and irrotational flow only and therefore flow separation was not predicted. Webber et al. (2011) performed a study of the flow over a flipper, using RANS numerical model applying the Spalart-Allmaras and the k-omega SST turbulence models. The authors concluded that severe inaccuracies were identified in the post stall regime, thereby raising question of the suitability of either one or two-equation turbulent models for this problem. Skillen et al. (2015) numerically investigated the performance of a tubercled airfoil using a Large Eddy Simulation (LES) model. The study showed a positive correlation on the aerodynamic forces, however, the study was conducted for only one angle of attack and therefore it is difficult to determine the accuracy of the setup for the whole range of angles of attack. Pedro et al.(2008) and Ming Zhao (2017) carried out Detached Eddy Simulations (DES) in a transitional regime of a similar configuration and found reasonable agreement with experiments, where the differences were around a 4% when compared to the experiments.

While to date research has focused on the performance of tubercled foils in laminar, transitional and a near-turbulent flow regimes, a fully turbulent flow regime has not been investigated. Even though it is expected that the tubercled hydrofoils would be beneficial if applied at very high Reynolds numbers, this has not been confirmed in the literature. For that reason, the research presented in this paper focuses on the investigation of the behaviour of leading edge tubercled foils in a fully turbulent flow regime. Author's particular interest is to understand if this technology may be successfully applied in ship design to improve a ship's hydrodynamic performance.

In order to achieve the specified aim, a range of numerical simulations is conducted using computational fluid dynamics to analyse the hydrofoil's flow structure and hydrodynamic performance. The physical case under review is a NACA 634_{021} hydrofoil with and without leading edge tubercles. This model was chosen due to previously

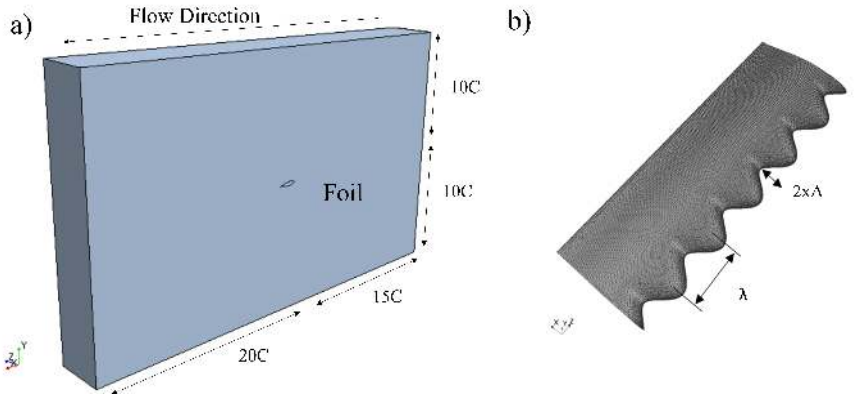

FIGURE 1. (a) Virtual towing tank showing the foils location (b) Isometric view of the meshed tubercled foil

conducted hydrodynamic experimental work (Johari et al., 2007); this case was assessed in a transitional flow regime at a Reynolds Number of $1.8\text{x}10^5$. The results from the experiments are used to validate the quality of the CFD setup. Once the numerical model was validated, the hydrofoils behaviour in the turbulent regime was assessed against lift, drag, vorticity fields and compared with its behavior when operating in a transitional regime.

2. Foil Geometry and Investigation Cases

The hydrofoil under investigation is a NACA 634_{021} without (baseline) and with leading edge tubercles that are defined by a mean chord (C) of 100mm and 300mm span (s) (see figue 1b). The geometry of the leading edge with tubercles is modeled as a sinusoid $X_{LE} = A\ sin(\lambda z)$, with an amplitude $A = 0.1xC$ and a wavelength $\lambda = \frac{2\pi}{0.5C}$.

The hydrofoils were investigated at a chord length based Reynolds Numbers of $1.83\text{x}10^5$ (transitional regime corresponding to the experiments) and $1\text{x}10^7$ (turbulent regime) and for a range of the Angles of Attack (AoA) of 0 to 30° in 5° interval. The foil model was placed in a prismatic virtual tank that corresponds to the experiments (Johari et al., 2007) as shown in the figure 1a.

3. Numerical Method

As this problem represents an incompressible viscous flow around a symmetrical body, the phenomenon can be numerically simulated by a computational fluid dynamics (CFD) code. In this study the commercial software Siemens STAR-CCM+ was used.

A significant effort was focused on applying the appropriate turbulence model. An initial numerical investigation was conducted applying the RANS code with the SST Menter turbulent model. However, as in Webber et al. (2011), the computed results were not comparable with experimental results. The reason why this methods cannot precisely calculate fluid variables is because the fluid velocity and pressure are time averaged, which leads to an inaccurate prediction of the flow separation that is of essential importance for this case. To overcome this issue, an Improved Delayed Detached Eddy Simulations (IDDES) model was applied as it is able to capture the large eddies present in the simulations. In general, this model is a hybrid switching between RANS with the SST k-Omega model, in the region near the non-slip wall, and the LES method in the wake

region. The Detached Eddy Simulation (DES) formulation of the SST K-Omega model developed by Shur *et al.* (2008) is obtained by modifying the dissipation term of the transport equation for the turbulent kinetic energy (k). After introducing a length scale, L_{hybrid} , the turbulent model equations in tensor form are given as:

$$\frac{\partial(\rho k)}{\partial t} + \frac{\partial(u_j k)}{\partial x_j} = \frac{\partial}{\partial x_j}\left[(\mu_l + \sigma_k \mu_t)\frac{\partial k}{\partial x_j}\right] + \tau_{ij} S_{ij} - \frac{\rho k^{3/2}}{L_{hybrid}} \tag{3.1}$$

$$\frac{\partial(\rho\omega)}{\partial t} + \frac{\partial(\rho u_j \omega)}{\partial x_j} = \frac{\partial}{\partial x_j}\left[(\mu_l + \sigma_\omega \mu_t)\frac{\partial \omega}{\partial x_j}\right] + \alpha\frac{\omega}{k}\tau_{ij} S_{ij} - \frac{\rho k^{3/2}}{L_{hybrid}} - \beta\rho\omega^2 + 2(1 - F_1)\frac{\rho\sigma_{\omega 2}}{\omega}\frac{\partial k}{\partial x_j}\frac{\partial \omega}{\partial x_j} \tag{3.2}$$

where S_{ij} represents the strain tensor,$\tau_{ij}$the stress tensor, $F_1$is the blending function. The length scale, L_{hybrid} is defined as follows:

$$L_{hybrid} = f_B(1 + f_e) L_{RANS} + (1 - f_B) L_{LES} \tag{3.3}$$

where $L_{RANS} = k^{\frac{1}{2}}/(\beta^*\omega)$, β^* is given in k-Omega Model Coefficients taken as 0.09. $L_{LES} = C_{DES}\Delta$, being $C_{DES} = 0.78$, and Δ is the grid length scale. The elevating-function f_e prevents an excessive reduction of the RANS Reynolds Stresses (Shur et al., 2008). The key of this model is the empirical blending-function, f_B , which presents a switching function from RANS ($f_B = 1$) to LES model ($f_B = 0$).

The transport equation for the turbulent kinetic energy in the regions where the fluid flow is modelled with the RANS SST Menter k-ω is insensitive to the stabilizing and destabilizing effects usually associated with strong (streamline) curvature and frame-rotation. These effects are accounted for by using a curvature correction factor, which alters the turbulent kinetic energy production terms, G_k and G_ω, according to the local rotation and vorticity rates by a curvature correction factor f_c (Arolla et al., 2013). This correction factor is a function of the strain rate tensor and the rotation-rate tensor. More details of this model can be found in Arolla et al. (2013)

4. CFD Setup

The same setup was applied for both geometries: the baseline and tubercled foil.

The first set of simulation was done for the transitional flow regime in order to validate the numerical modelling method against experimental results. The numerical model was setup to replicate the conditions from the Johari's experiment. The upstream inlet is modelled using the velocity inlet condition whereas the downstream boundary is set to be the pressure outlet at a distance of 15 and 20 chord lengths from the hydrofoil respectively (Figure 1a). Initial levels of turbulence within the flow are prescribed. A sensitivity analysis was conducted for the turbulence inlet condition and chosen to be a 1%.

An upwind discretisation scheme that yields a second-order spatial accuracy was used for all flow variable calculations, with a convergence target of $1\text{x}10^{-6}$. In order to select an appropriate time step and ensure the simulation convergence, the Courant-Friedrichs-Lewy (CFL) condition was used, achieving a mean Courant number of 0.6.

In addition, the foil hydrodynamic force coefficients were used to monitor the convergence during the unsteady CFD simulations. These coefficients are defined as $C_L =$

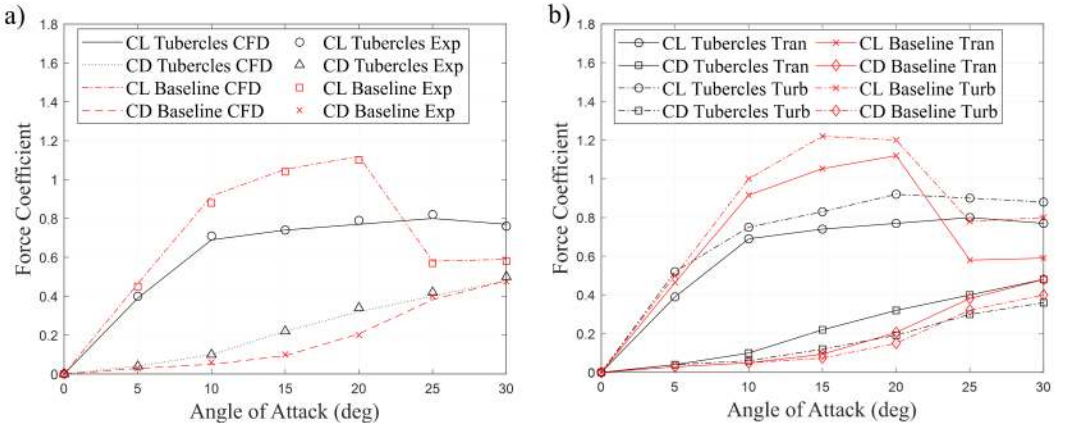

FIGURE 2. (a) Comparison of the lift and drag coefficient between CFD and experiments in transitional regime (Johari et al., 2007), (b) Numerical result for lift and drag coefficients in transitional and turbulent flow regime for the range of angles of attack

Mesh Name	Million Elements	C_L	C_D	Δ C_L (%)	Δ C_D (%)
1. Coarse	5.6	0.83	0.37	5.06	8.82
2. Medium	8.9	0.77	0.33	-2.53	-2.94
3. Fine	12	0.78	0.34	-1.27	-1.47
Experiments	-	0.79	0.35	-	-

TABLE 1. Mesh independence study at 20° AoA at a Re=1.83x10^5

$\frac{L}{\frac{1}{2}\rho\ U^2 S}$ and $C_D = \frac{D}{\frac{1}{2}\rho\ U^2 S}$ respectively, being L the lift force, ρ is the fluid density, U is the flow speed, S is the hydrofoil surface area, and D the drag force.

The domain was discretised with a hexagonal mesh, combined with prism layers at solid boundaries with y+ value of less than 1. A mesh independence study was conducted for three mesh sizes: coarse (1), medium (2) and fine (3) with a refinement ratios of $r_{21} = 1.26$ and $r_{31} = 1.46$, respectively. It was found that the lift and drag coefficients obtained with the medium and the fine mesh are very close and comparable with the experimental results; the medium mesh was within 3% and the fine mesh within 2% of the experimental results as presented in table 1. Therefore, the fine mesh, with 12 million elements was selected as the most suitable for this study.

A turbulent regime simulation case was developed based on the baseline case described above. A mesh sensitivity study was conducted for the turbulent flow regime, using three meshes: 11M, 12M and 13M elements, confirming that the adopted baseline setup with fine mesh was appropriate for the turbulent flow regime.

5. Results Analysis

5.1. *Validation*

Experimental lift and drag coefficients obtained by Johari et al. (Johari et al., 2007) were used to validate the setup in the transitional flow regime. In figure 2a, a comparison

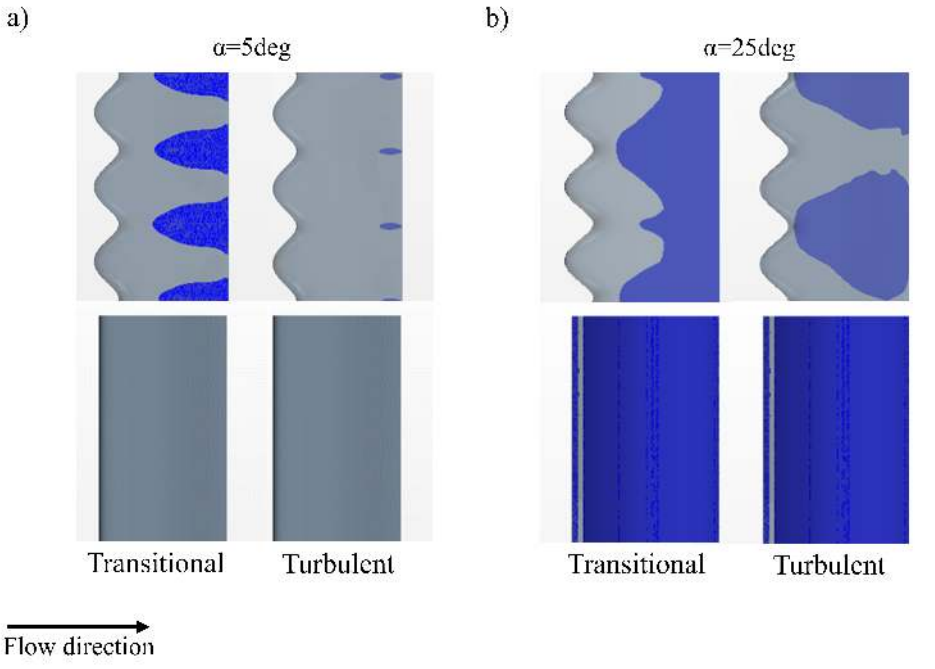

FIGURE 3. (a) Plan view of the hydrofoil suction side showing (blue) flow separation in transitional (left) and turbulent (right) flow regimes for the tubercled and baseline foils at 5° AoA. (b) Plan view of the hydrofoil showing (blue) flow separation in transitional (left) and turbulent (right) flow regimes for the tubercled and baseline foils at 25° AoA.

is shown between the experimental and numerical (CFD) lift and drag coefficients for the baseline and tubercled foils. Overall, the numerically predicted coefficients correlate very well with the experimental results in transitional regime. The results show that for the baseline foil, the lift coefficient increases rapidly from 0 to 10deg AoA, and steadily until 20deg, where stall occurs and C_L substantially drops. When looking at the tubercled foil, it can be seen that in transitional regime at low angles of attack its behaviour is worse than the baseline foil. However, once the baseline foil reaches the stall angle, the tubercled foil is able to maintain a nearly constant lift without stall occurring.

The CFD simulations were able to catch the same trend of lift and drag curves across the range of angles of attack, with an excellent level of deviation of 2% only. Therefore, the adopted numerical model and mesh refinement were adopted as a baseline setup for the further study in transitional and turbulent flow.

5.2. *Hydrodynamic Performance*

Figure 2b shows the calculated lift and drag coefficients for both hydrofoils, the tubercled and the baseline, comparing their performance in turbulent and transitional flow regimes. Figure 3 shows flow separation pattern for both hydrofoils and in both flow regimes at two angles of attack, 5deg (figure 3a: pre stall) and 25deg (figure 3b: post stall). The regions of a negative shear stress in streamwise direction are shaded, indicating the occurrence of the flow separation.

The coefficients for the baseline foil (figure 2b) demonstrate the similar trends in turbulent and in transitional flow regimes. The lift coefficient C_L increases rapidly from 0 to 10deg AoA, and steadily until 20deg, when the stall occurs and C_L rapidly drops.

This is consistent with the flow separation captured in figure 3. At small AoA the baseline foil shows no flow separation in both regimes. However, at post stall AoA (25deg), the flow on the suction side is completely separated. In regard to the drag coefficient, C_D increases continuously troughout the range of AoA, with slightly lower values in turbulent regime.

In case of the tubercled foil, the performance in transitional and turbulent flow are comparable as the curves have a similar trend, with C_L and C_D increasing throughout the whole range of AoA (figure 2b). However, the performance in turbulent regime is better than in transitional with higher C_L and lower C_D trough the whole range of AoA. The flow separation is present in both regimes (figure 3). At low AoA, in transitional regime, it is observed that the separation occurs further upstream over the troughs rather than over the peaks (at around 1/3 of the chord). This is consistent with the findings in the literature (Bolzon et al, 2015; K.L. Hansen, 2012; Miklosovic et al., 2004; N. Rostamzadeh et al, 2014). Additionally, a laminar separation bubble is identified at the leading edge of the troughs in transitional flow regime (as shown at the isometric view in figure 4). Figure 3 shows that the level of flow separation on the suction side is lower in turbulent flow than in transitional for the whole range of AoA. At low AoA, the difference between the scale of the separation in transitional and turbulent flow is obvious. While in transitional flow significant areas of separation were identified behind each trough and developing further downstream, in turbulent flow separation close to the trailing edge is observed only in the very small regions further downstream. This confirms that in turbulent flow the separation is significantly suppressed and shifted further downstream compared with transitional flow. At high AoA, the flow separation is high however still below level captured in the transitional flow regime.

When comparing the performance in turbulent regime of the tubercled foil with the baseline one, it can be seen that at low angles of attack the tubercled foil behaviour is worse than the baseline foil (lower C_L and higher C_D). However, once the baseline foil reaches the stall angle and experiences a drop in C_L (around 20deg), the performance of the tubercled foil becomes superior as it is able to maintain C_L at approximately the same value while C_D is slightly reduced. This lower drag coefficient at large AoA is not achieved in transitional regime and is only specific for behaviour in turbulent flow regime.

In line with the results presented in figures 2 and 3, in can be concluded that in both regimes at pre-stall AoA, the baseline foil performs better than the tubercled foil as flow separation does not occur. In contrast, at post stall AoA, the tubercled foil performs superior as level of flow separation is lower than for the baseline foil where the flow separation occurs across a whole suction side.

5.3. *Tubercles Mechanisms of Action*

This study confirmed that the fundamental leading edge tubercles mechanism of action that researchers encountered in transitional and laminar flow regime is present in turbulent flow regime as well. The first feature is the existence of 3D streamwise counter-rotating pair of vortices formed over each tubercle peak. These vortex structures are confirmed by positive isosurfaces of Q criterion $Q = \frac{1}{2}\left(\Omega_{ij}\Omega_{ij} - S_{ij}S_{ij}\right)^{\frac{1}{2}}$, where Ω is the rotation tensor and S is the strain tensor (Hussain et al, 1995). The identified 3D vortices are shown in the figure 5a and are generated due to the difference in pressure that exists between the pressure and suction faces of a hydrofoil's peaks. They are created due to the flow's tendency to travel from the high pressure to the low pressure regions of the hydrofoil (figure 5b). The size of the counter-rotating vortices gradually increases, mixing the upper regions of the boundary layer as shown in the figure 5c. This phenomenon is

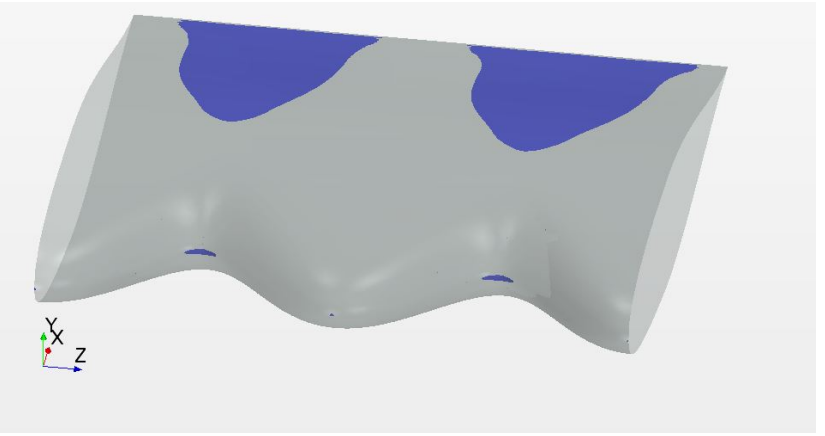

FIGURE 4. Isometric view of the foil showing the laminar separation bubble over the leading edge of the tubercled foil in transitional regime at 5°AoA

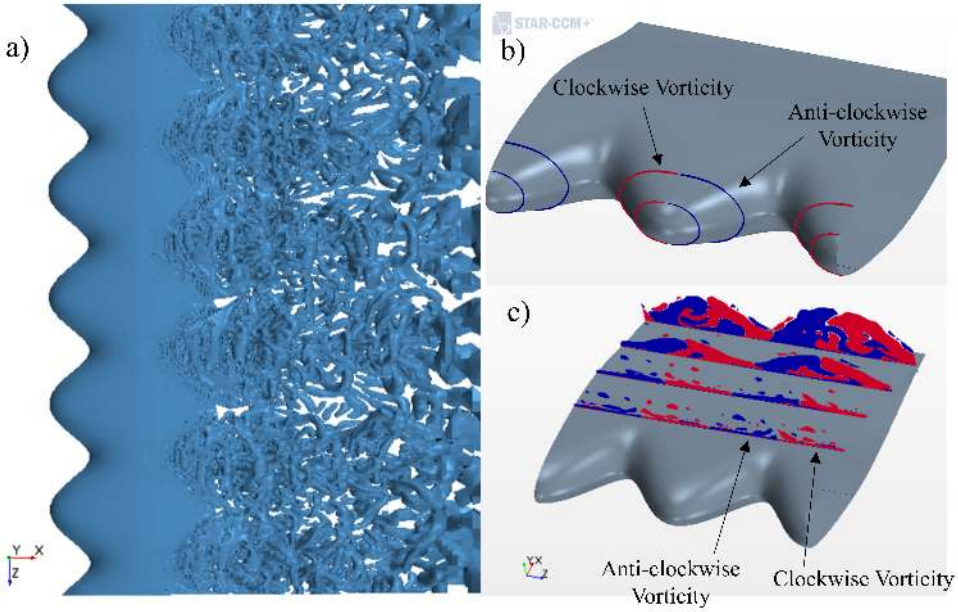

FIGURE 5. (a) Instantaneous isosurfaces of Q criterion (b) and (c) Evolution of the streamwise vorticity at different chord locations at 10° AoA in turbulent regime

seen at all angles of attack, being weaker at lower angles of attack as expected and it is consistent with the literature (N. Rostamzadeh et al., 2014; Skillen et al, 2015).

The second feature observed in the turbulent regime is a cyclic variation of the pressure in the spanwise direction, resulting in the depression areas behind the troughs on the suction side of the hydrofoil (figures 6 and 7). These pockets of low pressure (white regions) direct the fluid to travel spanwise from the zones of high pressure (peaks) to the zones of low pressure (troughs), leading to the formation of a secondary spanwise flow. As shown in the figure 6, this is manifested by the near-wall streamlines being squeezed from the peaks towards the troughs. This finding is seen at low angles (figure 6) and high angles (figure 7) of attack and it is consistent with the observations in transitional

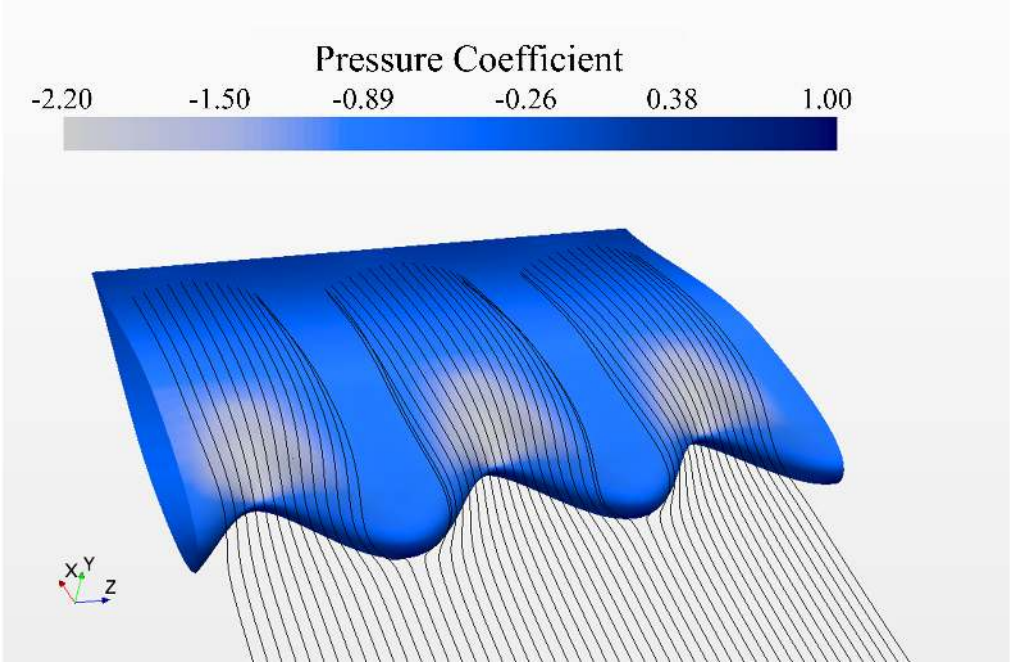

FIGURE 6. Suction side pressure distribution and near-wall time-averaged streamlines in turbulent flow at 5°AoA

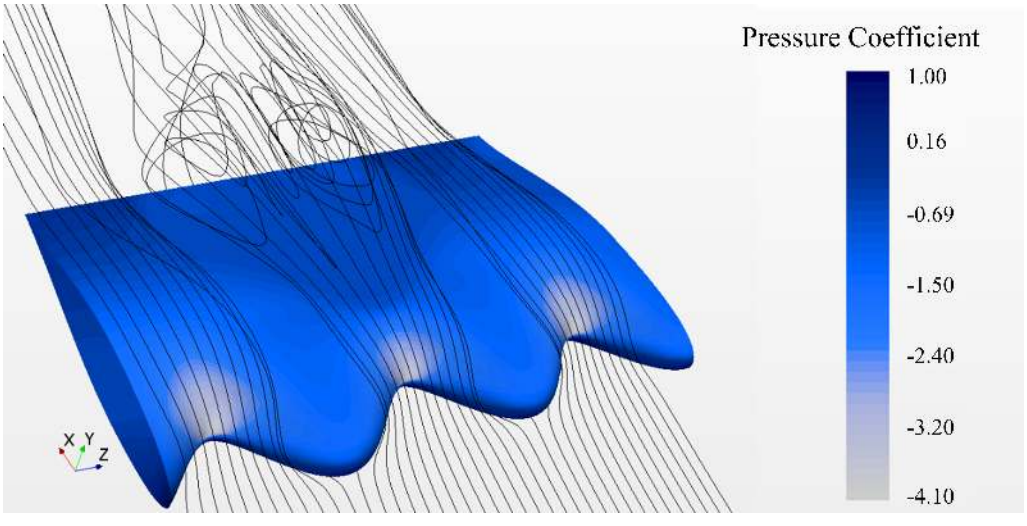

FIGURE 7. Suction side pressure distribution and near-wall streamlines in turbulent flow at 25°AoA

and laminar flow regimes (N. Rostamzadeh et al., 2014; Nikan Rostamzadeh et al., 2017; Skillen et al, 2014). Due to this secondary flow, the low momentum fluid particles that lie next to the wall are deflected and transported away from the peaks towards the troughs (Skillen et al., 2015). The near-wall region over the peaks (figure 6 an 7 gap in streamlines pattern), is filled with higher momentum fluid that is transported down from the upper region of the boundary layer, explaining why the first occurrence of separation is located behind the troughs (figure 3).

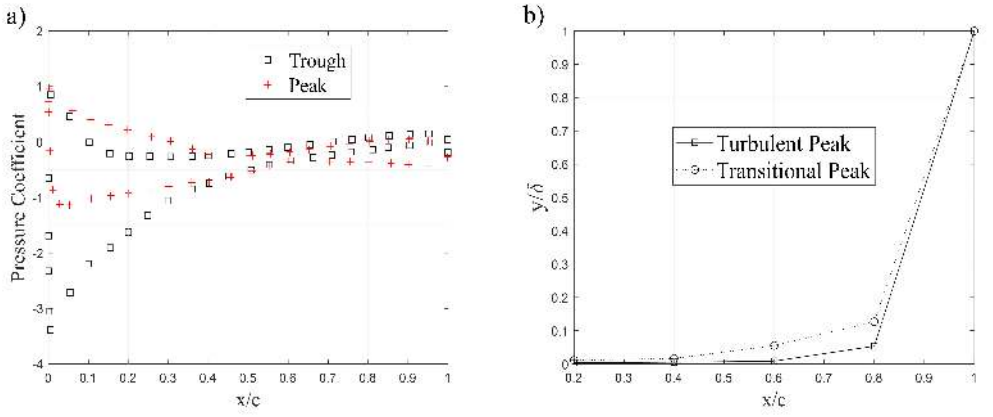

FIGURE 8. (a) Pressure distribution along the chord at 10°AoA in the turbulent flow regime. (b) Peak's boundary layer thickness on different locations along the chord at 10°AoA

The existence of the minimum pressure at the troughs and spanwise pressure differences as shown in figure 6 is also confirmed by the pressure distribution along the chord (presented in figure 8a). These two curves are measured at the center-most peak and trough. Small spanwise pressure variations within a 1-2% are measured at low AoA. High AoA pressure distribution over the two sets of peaks and troughs shown in figure 7 are presented in the figure 9. From the pressure distribution it is clear that consecutive troughs present a different pressure distribution along the suction side of the hydrofoil. This is due to vortex interactions or the 'bi-periodic phenomenon' already reported in experiments (Johari et al, 2007) and numerical studies (Zhao et al, 2017).

In addition, figure 8a shows a spanwise variation of the pressure at all angles of attack, the minimum pressure is developed over the suction side troughs. The same phenomenon is identified in laminar and transitional flow regimes and are consistent with the literature (Hansen, 2012). This pressure variation is caused by the difference in chord lengths at peaks and troughs together with the curved shape of the foil that drives the vortices to migrate towards the trough and form low pressure regions. As a consequence, the bulk of the flow is directed behind the chord minima (troguhs). As a consequence, strong flow acceleration behind the troughs causes a consequential local augmentation of the minimum suction pressure (Skillen, 2015).

This flow pattern causes changes in the boundary layer as well. Figure 8b presents the boundary layer thickness along the peak's chord for transitional and turbulent flow. As expected, with an increase in Reynolds number the boundary layer is getting thinner. This difference in the thickness of the boundary layers has been seen across the whole range of angles of attack under consideration.

For the tubercled foil, this thinning phenomenon is more pronounced due to a combination of the mixing mechanism as part of the vortex generation and second mechanism of influx of the higher momentum fluid particles from upper region of the boundary layer into the near-wall region. This phenomenon does not conflict with the control mechanisms of action of the tubercled foil. Instead, it amplifies the generation of the large 3D vortices, improving the hydrodynamic performance of the hydrofoil overall.

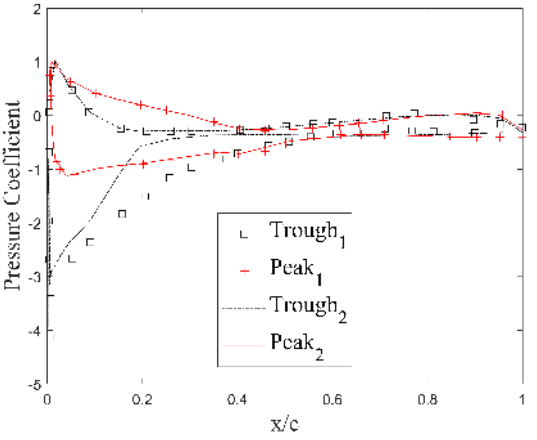

FIGURE 9. Pressure distribution along the chord at 25°AoA in the turbulent flow regime.

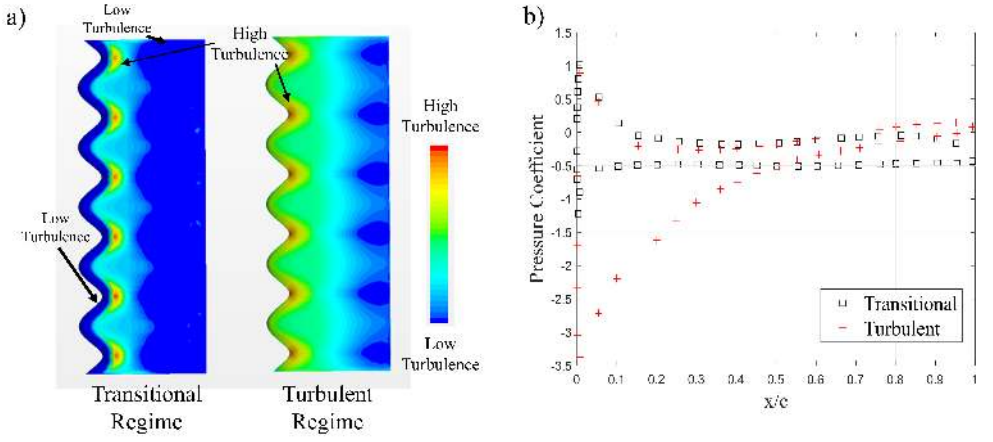

FIGURE 10. Turbulent kinetic energy on the suction side at 10°AoA. (b) Trough pressure distribution at 10°AoA in turbulent and transitional flow regime

5.4. *Development of Turbulence*

Figure 10a shows a turbulent kinetic energy (k) field in the near-wall region for the transitional and turbulent flow regimes. The regions coloured in blue (dark and light) indicate the zones of a low turbulence where the flow is mostly laminar, whereas regions coloured in yellow and red indicate the zones where the turbulent flow is developing. In transitional flow regimes, there is a small region along the leading edge that sees a laminar flow (dark blue region) before the transition to turbulent flow takes place, followed further downstream by flow separation (blue region again). In contrast, in the turbulent regime, the turbulent boundary layer is energized further upstream than in the transitional flow regime and a high turbulent kinetic energy is seen immediately behind the troughs, near the wall. This is caused by the high velocity gradients that are formed as the near-wall flow moves from the peak to the trough. This explains why the hydrofoil in the turbulent flow regime experiences less flow detachment.

Another observation that explains why the troughs experience less detachment in the turbulent flow regime can be made from the pressure distribution presented in figure

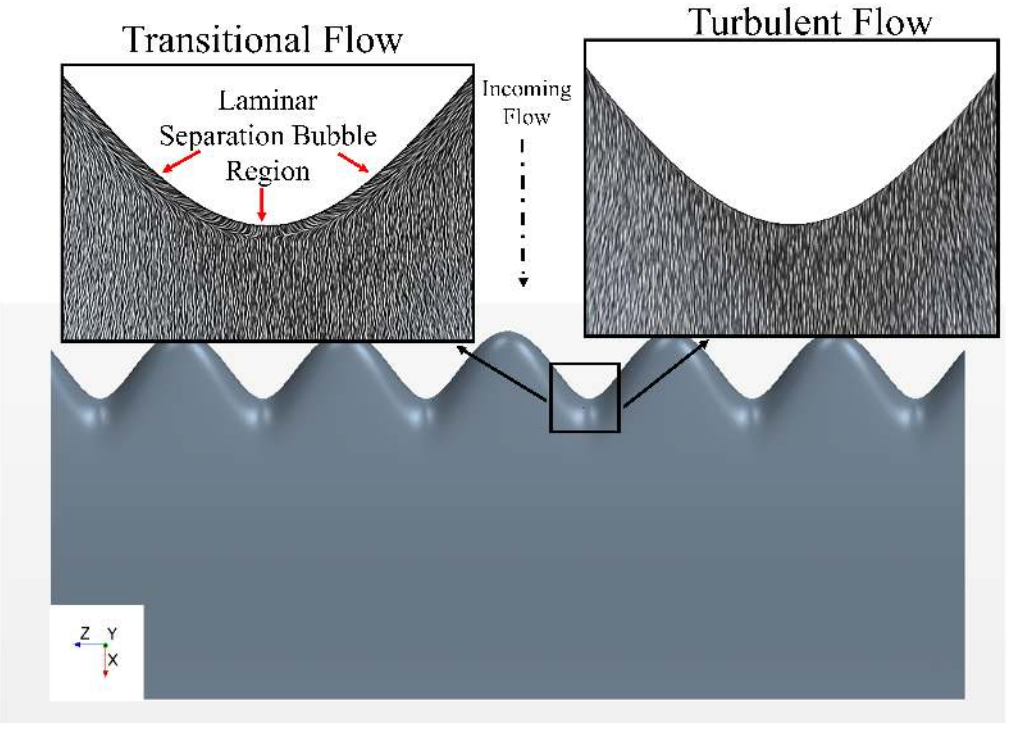

FIGURE 11. Shear stress plotted using the line integral convolution technique at 5°AoA for transitional and turbulent flow regimes

10b. In transitional flow regime, the pressure on the leading edge of the suctions side increases instantly while in turbulent flow regime, the pressure increases gradually. As a result, in transitional flow regime a laminar separation bubbles are formed at leading edge on troughs, whereas in the turbulent flow regime, the formation of the separation bubble is suppressed together with its detrimental effects (drag and separation). This is further confirmed by the wall shear stress distribution on the suction side of the foil shown in figure 11. In the transitional flow regime, near the leading edge, the region of the laminar separation bubble is identified (left-hand inset) whereas right-hand inset shows that in turbulent flow regime, the laminar separation bubble does not exist. This is an important finding, not previously reported in literature, that extends our understanding of the turbecled foil performance in turbulent flow.

6. Conclusions

This research confirms that the behavior of the turbecled hydrofoils in turbulent flow regime is consistent to phenomena identified in transitional flow regime for incompressible fluid. When comparing turbecled with smooth baseline hydrofoil, analysis confirmed that, at pre-stall angles of attack, the baseline hydrofoil performs better than the tubercled in all turbulent and transitional flow regimes. However, in post stall conditions, when baseline performance suddenly drops, the tubercled foil becomes superior due to the lower level of flow separation, increased lift and lower drag coefficients.

The main mechanism of action of a tubercled hydrofoil in the turbulent flow, is the formation of the pairs of counter-rotating streamwise vortices mixing a near-wall, low

momentum flow with a higher momentum flow from the upper region of the boundary layer. This phenomenon is combined with the appearance of the secondary flow in a spanwise direction caused by the pressure difference behind peaks and troughs. In turbulent flow regime, at lower angles of attack the flow separation on the suction side is significantly suppressed, as well as laminar separation bubble that, in transitional flow regime, exists on the leading edge of troughs. In addition, for the tubercled hydrofoil in turbulent flow regime, the study identified a phenomenon of thinning of the boundary layer that takes place, further delaying the stall. This phenomenon does not conflict with the principal tubercles mechanism of action. On contrary, it contributes to more stable mixing of the vortices and improves the overall hydrodynamic performance of the foil.

This numerical modeling approach that is able to capture the tubercled hydrofoil action in sufficient detail is recommended as part of systematic analysis of the turbecles hydrofoil devices and their design. This is of significant importance when looking in potential application on ships and it would replace the commonly used practice where expensive physical testing is needed to assess the ship efficiency and identify further design iterations required.

The importance of this study is that it gives in-depth insight in the complex mechanism of action of the tubercled hydrofoil over the whole range of flow regimes and angles of attack. This work contributes to knowledge required to investigate the potential applications of the tubercles as hydrodynamic flow control devices.

As a future work, it would be beneficial to confirm the findings presented in this paper with a comprehensive experimental investigation of the tubercled hydrofoil in an incompressible, fully turbulent flow regime. In addition, it is recommended to investigate how the tubercles geometry parameters impact on the thinning of the boundary layer and 3D vortex generation phenomena. These further work would allow to better predict and control flow behavior and identify potential future flow control technology applications.

REFERENCES

Arolla, S. K., & Durbin, P. A. (2013). Modeling rotation and curvature effects within scalar eddy viscosity model framework. International Journal of Heat and Fluid Flow.

Bolzon, M. D., Kelso, R. M., & Arjomandi, M. (2015). Tubercles and Their Applications. Journal of Aerospace Engineering.

Fish, F. E., & Battle, J. M. (1995). Hydrodynamic design of the humpback whale flipper. Journal of Morphology.

Hansen K.L., K. R. M. & D. B. B. (2009). The effect of leading edge tubercle geometry on the performance of different airfoils.

Hansen, K. L. (2012). Effect of leading edge tubercles on airfoil performance. PhD Thesis. School of Mechanical Engineering. University of Adelaide.

Hussain, F., Jeong, J. (1995). On the identification of a vortex. Journal of Fluid Mechanics, 285, 69–94. DOI: https://doi.org/10.1017/S0022112095000462

Johari, H., Henoch, C., Custodio, D., & Levshin, A. (2007). Effects of leading-edge protuberances on airfoil performance. AIAA Journal.

Miklosovic, D. S. Murray, M. M., & Howle, L. E. (2007). Experimental evaluation of sinusoidal leading edges. Journal of Aircraft.

Miklosovic, D. S., Murray, M. M., Howle, L. E., & Fish, F. E. (2004). Leading-edge tubercles delay stall on humpback whale (Megaptera novaeangliae) flippers. Physics of Fluids.

Murray, M. M., Miklosovic, D. S., Fish, F., & Howle, L. (2005). Effects of Leading Edge Tubercles on a Representative Whale Flipper Model at Various Sweep Angles.

Pedro, H. T. C., & Kobayashi, M. H. (2008). Numerical study of stall delay on humpback whale flippers. 46th AIAA Aerospace Sciences Meeting and Exhibit.

Rostamzadeh, N., Hansen, K. L., Kelso, R. M., & Dally, B. B. (2014). The formation mechanism

and impact of streamwise vortices on NACA 0021 airfoil's performance with undulating leading edge modification.

Rostamzadeh, N., Kelso, R. M., & Dally, B. (2017a). A numerical investigation into the effects of Reynolds number on the flow mechanism induced by a tubercled leading edge. Theoretical and Computational Fluid Dynamics.

Serson, D., Eneghini, J. R., & Herwin, S. J. (2017). Direct numerical simulations of the flow around wings with spanwise waviness. Journal of Fluid Mechanics.

Shi, W., Rosli, R., Atlar, M., Norman, R., Wang, D., & Yang, W. (2016). Hydrodynamic performance evaluation of a tidal turbine with leading-edge tubercles. Ocean Engineering.

Shur, M. L., Spalart, P. R., Strelets, M. K., & Travin, A. K. (2008). A hybrid RANS-LES approach with delayed-DES and wall-modelled LES capabilities. International Journal of Heat and Fluid Flow.

Skillen, A., Revell, A., Pinelli, A., Piomelli, U., & Favier, J. (2015). Flow over a Wing with Leading-Edge Undulations. AIAA Journal.

Stanway, M. J. (2008). Hydrodynamic effects of leading-edge tubercles on control surfaces and in flapping foil propulsion. Master of Science in Oncean Engineering.

Watts, P., & Fish, F. E. (2001). The influence of passive, leading edge tubercles on wing performance. Proc. Twelfth Intl. Symp. Unmanned Untethered Submers. Technol., Durham New Hampshire.

Weber, P. W., Howle, L. E., Murray, M. M., & Miklosovic, D. S. (2011). Computational Evaluation of the Performance of Lifting Surfaces with Leading-Edge Protuberances. Journal of Aircraft.

Zhao, M., Zhang, M., & Xu, J. (2017). Numerical simulation of flow characteristics behind the aerodynamic performances on an airfoil with leading edge protuberances. Engineering Applications of Computational Fluid Mechanics.